Numerical simulation of bubble collapse and the transfer of vapor and noncondensable gas through the bubble interface using the ghost fluid method

Y Jinbo[1*], K Kobayashi[1], M Watanabe[1] and H Takahira[2]
[1] Division of Mechanical and Space Engineering, Hokkaido University, Sapporo 060-8628, Japan
[2] Department of Mechanical Engineering, Osaka Prefecture University, Sakai 599-8531, Japan
[*] E-mail: jinbo_y@eng.hokudai.ac.jp

Abstract. The ghost fluid method is improved to include heat and mass transfer across the gas–liquid interface during the bubble collapse in a compressible liquid. This transfer is due to both nonequilibrium phase transition at the interface and diffusion of the noncondensable gas across the interface. In the present method, the ghost fluids are defined with the intention of conserving the total mass, momentum, and energy, as well as the mass of each component while considering the heat and mass fluxes across the interface. The gas phase inside the bubble is a mixture of vapor and noncondensable gas, where binary diffusion between the mixture components is taken into account. The gas diffusion in the surrounding liquid is also considered. This method is applied to a simulation of a single spherical bubble collapse with heat and mass transfer across the interface in a compressible liquid. When noncondensable gas is present, it accumulates near the interface due to vapor condensation, thereby preventing further condensation. This results in a weaker bubble collapse than the case without noncondensable gas.

1. Introduction

Significant research efforts have recently been devoted to applying the extremely high pressure and temperature fields derived from bubble collapse to new environments for medical application and for the synthesis of new materials [1, 2]. Hatanaka [2] measured the amount of OH radicals dissolving into liquid from a single bubble oscillating in ultrasonic fields and showed that the amount increases under the "dancing bubble condition," where a single bubble is not stably located while oscillating, but rather moves around accompanied with splitting and coalescing. To clarify the mechanism behind the increase, it is necessary to construct a computational method that can simultaneously treat both nonspherical bubble collapse accompanied by complicated interfacial structure and heat and mass transfer through the interface. Although many numerical simulations have been conducted until now [3-5], these methods are considered to be insufficient for computing violent bubble collapse yielding chemical reactions whilst considering both the complicated structure and the heat and mass transfer.

In this study, a numerical method for compressible two-phase flows is presented that can treat nonspherical bubble collapse with complicated deformation of the interface accompanied by heat and mass transfer through the interface (i.e., diffusion of noncondensable gas and nonequiliblium phase transition of vapor). In our previous studies [6, 7], nonequilibrium phase transition following nonspherical bubble collapse was considered by developing the ghost fluid method (GFM) [8]. In this study, this method is extended to treating heat and mass transfer due to diffusion of noncondensable gas through an interface, while simultaneously treating the nonequilibrium phase transition.

A similar method has been recently constructed to solve the pressure and velocity differences at the interphase due to phase transition by Houim & Kuo [9]; their method employs the idea of the modified

GFM [10] which applies the solution of two-phase Riemann problem to the definition of the ghost fluid. Their method is considered to solve certain situations more appropriately than our method just as the modified GFM is known to perform better than the original GFM [10]. Here, however, we adopt the original GFM because of the simplicity of extending it to the multidimensional problem.

2. Numerical methods

Although the following presents the construction of the spherical 1-D computational method, it can be straightforwardly extended to the multidimensional simulation and treatment of the complicated interfacial structure, because the present method is constructed by extending the level set method (LSM) [11] and the GFM [8] which are respectively used for implicitly capturing the location of the interface and implicitly satisfying the boundary conditions at the interface.

2.1. Governing equations

In the bubble interior, the Euler equations for the two species are solved with consideration for heat conduction and mutual diffusion of vapor and noncondensable gas. This is the same as in the computation of Matsumoto & Takemura [3] except that we neglect the fluid viscosity. For the bubble exterior, the Euler equations are solved; the distribution of the noncondensable gas dissolved in the liquid phase is obtained by solving the advection–diffusion equation with the velocity field of the liquid phase in a manner similar to the computation of Akhatov et al. [4]. The following stiffened gas equations of state [12] are employed for the noncondensable gas (air), the liquid (water), and its vapor:

$$p = (\gamma - 1)\rho(E - \epsilon) - \gamma\Pi, \qquad E = \frac{C_p}{\gamma}T + \frac{\Pi}{\rho} + \epsilon \tag{1}$$

where p is the pressure, ρ is the density, E is the internal energy per unit mass, T is the temperature and γ, Π, ϵ, C_p are the parameters for the characteristic of materials. The following values are used.

$$\text{water: } \gamma_l = 2.35, \Pi_l = 10^9 \text{ Pa}, \epsilon_l = -1167 \times 10^3 \text{ J/kg}, C_{pl} = 5.947 \times 10^3 \text{ J/(kgK)}$$
$$\text{vapor: } \gamma_v = 1.43, \Pi_v = 0 \text{ Pa}, \epsilon_v = 2030 \times 10^3 \text{ J/kg}, C_{pv} = 1.487 \times 10^3 \text{ J/(kgK)}$$
$$\text{air: } \gamma_g = 1.4, \Pi_g = 0 \text{ Pa}, \epsilon_g = 0 \text{ J/kg}, C_{pg} = 1.007 \times 10^3 \text{ J/(kgK)}$$

where subscript l, v and g represents the liquid, vapor and noncondensable gas, respectively.

Heat conduction obeys Fourier's law. The heat conductivity of each gas component linearly varies with temperature [13, 14]. The diffusion velocity is determined using Fick's law. The coefficient of binary diffusion of vapor and noncondensable gas is calculated using Fuller's equation [15]. The diffusion coefficient of noncondensable gas in liquid is $D_l = 1.76 \times 10^{-9}$ m^2/s [4]. The third-order TVD Runge–Kutta scheme and the third-order ENO-LLF scheme are used for time and space discretization of the Euler equations, respectively [16].

2.2. Numerical methods for gas–liquid interface

The boundary conditions imposed on the gas–liquid interface are almost the same as the ones used in [9]; in the present simulation, heat and mass fluxes due to the nonequilibrium phase transition, $\dot{m}_v$ (positive for evaporation), and due to the diffusion of noncondensable gas through the interface, $\dot{m}_g$ (negative for dissolution), are considered while the fluid viscosity is neglected.

2.2.1. Level set method [11]. The level set function φ is used for capturing the interface location. When mass transfer through the interface is neglected, the level set function is usually advanced by the advection equation with the fluid velocity fields. When a phase transition is considered, the distribution of velocities normal to the interface is discontinuous at the interface due to the phase transition. Therefore, the level set function is advanced using the modified velocity fields $\boldsymbol{u}_R$ as follows:

$$\boldsymbol{u}_R = \boldsymbol{u} - \frac{\dot{m}_g + \dot{m}_v}{\rho_m^i}\boldsymbol{n} \ (\varphi > 0: \text{gas phase}), \qquad \boldsymbol{u}_R = \boldsymbol{u} - \frac{\dot{m}_g + \dot{m}_v}{\rho_l^i}\boldsymbol{n} \ (\varphi < 0: \text{liquid phase}) \tag{2}$$

where $\boldsymbol{u}$ is the velocity vector, $\boldsymbol{n}(=\nabla\varphi/|\nabla\varphi|)$ is the unit normal, subscripts m represents the mixture, and superscript i means the value at the interface.

2.2.2. Ghost fluid method [8]. The GFM is used to prevent the fluid variables with discontinuous distributions across the interface from being numerically diffused. In the GFM, instead of explicitly applying the boundary conditions to the interface, the boundary conditions at the interface are implicitly satisfied by defining an artificial fluid (ghost fluid). The following definitions of the ghost fluid are obtained by extending the ghost fluid that is defined for modeling phase transitions to the treatment of the noncondensable gas diffusion through the interface.

$$
\begin{aligned}
&\boldsymbol{u}_m^{\text{ghost}}\cdot\boldsymbol{n}=\boldsymbol{u}_l^{\text{real}}\cdot\boldsymbol{n}-\frac{\dot m_g+\dot m_v}{\rho_l^i}+\frac{\dot m_g+\dot m_v}{\rho_m^i},\ p_m^{\text{ghost}}=p_m^{\text{ext}},\ s_m^{\text{ghost}}=s_m^{\text{ext}},\\
&\boldsymbol{u}_l^{\text{ghost}}\cdot\boldsymbol{n}=\boldsymbol{u}_l^{\text{ext}}\cdot\boldsymbol{n},\ p_l^{\text{ghost}}=p_m^{\text{real}}+\frac{\left(\dot m_g+\dot m_v\right)^2}{\rho_m^i}-\frac{\left(\dot m_g+\dot m_v\right)^2}{\rho_l^i}+\sigma\kappa,\ s_l^{\text{ghost}}=s_l^{\text{ext}},\\
&\boldsymbol{q}_m^{\text{ghost}}\cdot\boldsymbol{n}=\boldsymbol{q}_l^{\text{real}}\cdot\boldsymbol{n}-\dot m_vL_v-\dot m_gL_g+\frac{1}{2}\frac{\left(\dot m_g+\dot m_v\right)^3}{{\rho_l^i}^2}-\frac{1}{2}\frac{\left(\dot m_g+\dot m_v\right)^3}{{\rho_m^i}^2},\\
&\boldsymbol{q}_l^{\text{ghost}}\cdot\boldsymbol{n}=\boldsymbol{q}_m^{\text{real}}\cdot\boldsymbol{n}+\dot m_vL_v+\dot m_gL_g+\frac{1}{2}\frac{\left(\dot m_g+\dot m_v\right)^3}{{\rho_m^i}^2}-\frac{1}{2}\frac{\left(\dot m_g+\dot m_v\right)^3}{{\rho_l^i}^2},\\
&\left(\rho_g\boldsymbol{v}_g\right)_g^{\text{ghost}}\cdot\boldsymbol{n}=\frac{\rho_g}{\rho_m}\dot m_{\boldsymbol{v}}-\frac{\rho_v}{\rho_m}\dot m_g,\left(\rho_g\boldsymbol{v}_g\right)_l^{\text{ghost}}\cdot\boldsymbol{n}=\dot m_g-c^i(\dot m_g+\dot m_v)
\end{aligned}
\tag{3}
$$

where s is the entropy, σ is the surface tension, $\kappa(=\nabla\cdot\boldsymbol{n})$ is the curvature of the interface, $\boldsymbol{q}$ is the heat flux vector, $L_v(=h_v^i-h_l^i{:}\,h$ is the specific enthalpy) is the latent heat accompanying the phase transition of the vapor, $L_g(=h_g^i-h_l^i)$ is the latent heat related to the dissolution and volatilization of the noncondensable gas, and c is the concentration of the noncondensable gas dissolved in the liquid. The velocity of the mixture, $\boldsymbol{u}_m$, is the mass averaged velocity of each component and is related to the velocities of the individual components by $\boldsymbol{u}_g=\boldsymbol{u}_m+\boldsymbol{v}_g$ and $\boldsymbol{u}_v=\boldsymbol{u}_m+\boldsymbol{v}_v$, where $\boldsymbol{v}$ is the diffusion velocity. Superscripts "ghost," "real," and "ext" represent the ghost fluid value, the actual value at the point where the ghost fluid is defined, and the value extrapolated to the point from the other fluid across the interface, respectively. The ghost temperatures used for the calculation of $\boldsymbol{q}$ are defined considering the temperature jump, ΔT, due to the phase transition as follows:

$$
T_m^{\text{ghost}}=T_l^{\text{real}}-\Delta T,\qquad T_l^{\text{ghost}}=T_m^{\text{real}}+\Delta T \tag{4}
$$

Although the mass flux can be determined from any phase transition model, the Hertz–Knudsen–Langmuir model [4] (with the accommodation coefficient of 0.055) is employed in this work. The temperature jump is determined by an equation derived from molecular gas dynamics [17]. The mass flux due to the noncondensable gas diffusion through the interface is determined as follows:

$$
\dot m_g=D_l\left(c_l^i-c_{sat}\right),\qquad c_{sat}=H_np_g^i \tag{5}
$$

where H_n is Henry's law constant with the value of 1.481×10^{-10} Pa^{-1} [4].

3. Numerical results

The result obtained from the present method was compared with Fig. 7 in Matsumoto & Takemura [3]. It was confirmed that the present result was in good agreement with Matsumoto & Takemura.

Examples of the spherical symmetric computation are shown where a single vapor bubble containing a small amount of noncondensable gas collapses. Initial conditions are as follows: water pressure surrounding the bubble, p_0, is 0.1013 MPa; water density, ρ_{l0}, is 989.0 kg/m^3; initial temperature in the computational domain, T_0, is 296 K; and initial bubble radius, R_0, is 1 mm. Initially, the mass fraction of the mixture inside the bubble is spatially uniform and is equal to $\phi_0(=\rho_g/(\rho_g+\rho_v))$. The

mass fraction is set to 0 (only vapor), 0.02, 0.05, and 0.1 in the following computations. Initial vapor pressure, p_{v0}, is the saturation pressure at temperature T_0. In the present simulation, adaptive zonal grids with 10 layers (where the finest grid spacing is $7.8125\times10^{-5}R_0$) is applied according to the bubble radius. The length of the computational domain is $200R_0$ in the radial direction. Symmetric boundary conditions are used at the origin of the spherical coordinates, and nonreflective boundary conditions are applied at the edge of the computational region.

Figure 1 presents the time histories of (a) bubble radii and (b) total mass of vapor inside the bubble, $\overline{M_v}$. Enlarged view of a specific time period is shown in the inset at the right-hand side of each figure. The four lines represent the data obtained for different initial mass fraction. After the bubbles oscillate for several periods, the energy of oscillation is dissipated and the bubbles stabilize at a certain radius when the bubbles contain a small amount of noncondensable gas. On the other hand, when the bubble contains only the vapor ($\phi_0 = 0$), the entire vapor is transformed into liquid due to condensation.

4. Conclusion

We demonstrated improved LSM and GFM to treat the gas–liquid interface followed by the diffusion of the noncondensable gas through the interface and the nonequilibrium phase transition. The spherical bubble collapse accompanied by the heat and mass fluxes through the bubble interface was reasonably simulated.

References

[1] Umemura S, Kawabata K and Sasaki K 2007 *Elect. Commun. Japan Part III* **90** 63
[2] Hatanaka S 2011 *Proc. Symp. Ultrasonic Electronics (Kyoto, 8-10, Nov. 2011)* vol 32 p 41
[3] Matsumoto Y and Takemura F 1994 *JSME Int. J.* B **37** 288
[4] Akhatov I, Lindau O, Topolnikov A, Mettin R, Vakhitova N and Lauterborn W 2001 *Phys. Fluids* **13** 2805
[5] Szeri A J, Storey B D, Pearson A and Blake J R 2003 *Phys. Fluids* **15** 2576
[6] Jinbo Y and Takahira H 2012 *Trans. Jpn. Soc. Mech. Eng.* B **78** 1302
[7] Jinbo Y, Ogasawara T and Takahira H 2015 *Exp. Therm. Fluid Sci.* **60** 374
[8] Fedkiw R, Aslam T, Merriman B and Osher S 1999 *J. Comput. Phys.* **152** 457
[9] Houim R W and Kuo K K 2013 *J. Comput. Phys.* **235** 865
[10] Liu T G, Khoo B C and Yeo K S 2003 *J. Comput. Phys.* **190** 651
[11] Sussman M, Smereka P and Osher S 1994 *J. Comput. Phys.* **114** 146
[12] Saurel R, Petitpas F and Abgrall R 2008 *J. Fluid Mech.* **607** 313
[13] Prosperetti A, Crum L A and Commander K W 1988 *J. Acoust. Soc. Am.* **83** 502
[14] Spencer B B, Wang H and Anderson K K 2000 *Oak Ridge National Laboratory/TM-2000* **285**
[15] Fuller E N, Schettler P D and Giddings J C 1966 *Ind. Eng. Chem.* **58** 18
[16] Shu C -W and Osher S 1989 *J. Comput. Phys.* **83** 32
[17] Nigmatulin R I 1991 *Dynamics of Multiphase Media* vols 1 and 2 (New York: Hemisphere)

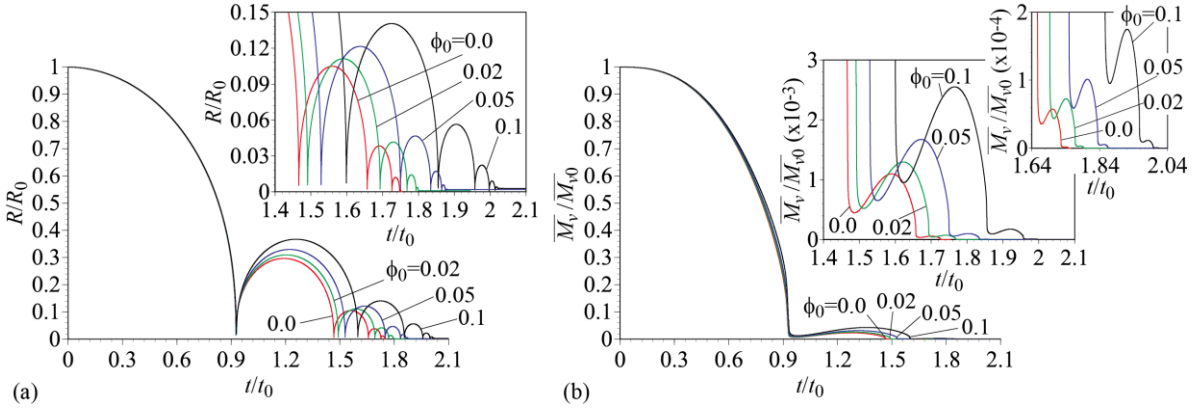

Figure 1. Time histories of (a) bubble radii and (b) total mass of vapor.